Advance Access publication on October 6, 2007

Cross-platform gene expression signature of human spermatogenic failure reveals inflammatory-like response

Andrej-Nikolai Spiess[1,†], Caroline Feig[1,†], Wolfgang Schulze[1], Frédéric Chalmel[2], Heike Cappallo-Obermann[1], Michael Primig[2,3] and Christiane Kirchhoff[1,4]

[1]Department of Andrology, University Hospital Hamburg-Eppendorf, Hamburg, Germany; [2]Biozentrum, Swiss Institute of Bioinformatics, Basel, Switzerland; [3]Present address: GERHM-INSERM U. 625, Groupe d'Etude de la Reproduction chez l'Homme et les Mammifères, University of Rennes 1, Rennes, France

[4]Correspondence addressed. Tel: +49-40-42803-1580; Fax: +49-40-42803-1554; E-mail: c.kirchhoff@uke.uni-hamburg.de

BACKGROUND: The molecular basis of human testicular dysfunction is largely unknown. Global gene expression profiling of testicular biopsies might reveal an expression signature of spermatogenic failure in azoospermic men. METHODS: Sixty-nine individual testicular biopsy samples were analysed on two microarray platforms; selected genes were validated by quantitative real-time PCR and immunohistochemistry. RESULTS: A minimum of 188 transcripts were significantly increased on both platforms. Their levels increased with the severity of spermatogenic damage and reached maximum levels in samples with Sertoli-cell-only appearance, pointing to genes expressed in somatic testicular cells. Over-represented functional annotation terms were steroid metabolism, innate defence and immune response, focal adhesion, antigen processing and presentation and mitogen-activated protein kinase K signalling pathway. For a considerable proportion of genes included in the expression signature, individual transcript levels were in keeping with the individual mast cell numbers of the biopsies. When tested on three disparate microarray data sets, the gene expression signature was able to clearly distinguish normal from defective spermatogenesis. More than 90% of biopsy samples clustered correctly into the corresponding category, emphasizing the robustness of our data. CONCLUSIONS: A gene expression signature of human spermatogenic failure was revealed which comprised well-studied examples of inflammation-related genes also increased in other pathologies, including autoimmune diseases.

Keywords: testis; interstitium; mast cells; microarray; distance-weighted-discrimination

Introduction

Male infertility is a major health problem affecting 15% of couples during their reproductive lifespan worldwide. Therapies are ineffective in a majority of the cases, and a growing number of patients undergo testicular biopsy for testicular sperm extraction (TESE) and ICSI into an oocyte. To date, histological examination of the biopsies is the only way to obtain diagnostic and prognostic information to devise appropriate medical treatment (for review, see Schulze *et al.*, 1999; McLachlan *et al.*, 2007). Sequencing of the human genome has profoundly affected the way in which pathologies are studied, spawning the development of high-throughput technologies such as gene expression profiling using high-density DNA microarrays. This method is now widely employed in the diagnosis of cancer and other potentially fatal human diseases (Alizadeh *et al.*, 2000; Bittner *et al.*, 2000; Perou *et al.*, 2000). Gene expression profiling is also likely to improve the diagnosis of male infertility and to promote individualized therapy design (He *et al.*, 2006).

To date, few studies have used global expression profiling to assess the molecular phenotypes of the normal and pathological human testis (Fox *et al.*, 2003; Rockett *et al.*, 2004; Yang *et al.*, 2004; Ellis *et al.*, 2007). However, in some of these publications the use of divergent grading systems, small biopsy numbers and pooling of samples make it difficult to interpret the results. Also, considering the heterogeneity of human testicular pathologies, the analysis of additional individual pathological and morphological subtypes is essential. We recently employed microarray analysis to reveal distinct subtypes of spermatogenic failure in humans (Feig *et al.*, 2007). In this approach, the selection of defined and histologically uniform subtypes, combined with the analysis of individual biopsy samples, was a crucial step. The pathological subtypes imply that the seminiferous tubules lack germ cells, and hence the corresponding cell type- and stage-specific transcripts, in a varying degree. We exploited this observation to reveal

[†]*A.N.S. and C.F. contributed equally.*

subtype-specific expression profiles which could be correlated with specific stages of human male germ cell development (Feig *et al.*, 2007). The vast majority of the differentially expressed transcripts were indeed testis- or even germ cell-specific, reflecting reduced numbers of the corresponding germ cells which normally express these mRNAs.

To reveal transcriptional changes occurring in testicular non-germ cells, we here focused on transcripts which increased during defective or absent spermatogenesis. These transcripts are likely to reflect changes in the somatic cells, and might reveal target genes for interventional therapy (for review, see He *et al.*, 2006). During routine diagnostic work-up of human testicular biopsies, the somatic cell types are often not further analysed because the focus is on germ cells. However, perturbed functions of Sertoli cells, peritubular myoid cells, interstitial Leydig cells and immune cells are known to accompany and may even cause spermatogenic failure. Infiltration of mast cells (Jezek *et al.*, 1999; Yamanaka *et al.*, 2000), interstitial fibrosis (Frungieri *et al*., 2002) as well as an altered distribution and/or dysfunction of Leydig cells (Tash *et al.*, 2002; Holm *et al.*, 2003; de Kretser, 2004; Andersson *et al.*, 2004) are frequently associated with testicular pathology (for review, see McLachlan *et al.*, 2007).

To be able to correlate the highly individual gene expression patterns of human testicular biopsies with distinct pathological subtypes, we analysed samples belonging to four frequently observed and uniform subtypes, termed 'normal spermatogenesis', 'uniform hypospermatogenesis', 'maturation arrest of germ cells at meiosis' and 'Sertoli-cell-only appearance'. Using two different oligonucleotide microarray platforms (Codelink and GeneChip arrays), we filtered 188 genes which showed significantly increased expression in the pathological subtypes, whereby the individual transcript levels increased with the severity of the pathology and also with the individual mast cell numbers of the biopsies. The validity of the gene expression signature was further confirmed by an integrated analysis of three independent microarray data sets. The molecular changes revealed hallmarks of a graded inflammatory-like response and might point to novel therapeutic targets.

Materials and Methods

Patients and testicular biopsies

Testicular biopsies were obtained from patients presenting at the Department of Andrology, University Hospital Hamburg-Eppendorf, Germany, between August 2004 and June 2006. Informed consent and Ethic Committee Approval was obtained (OB/X/2000), and the study conducted in accordance with the guidelines of the 'Helsinki Declaration'. Tissues were taken simultaneously for therapeutic TESE and diagnostic purposes as described previously (Jezek *et al.*, 1998; Schulze *et al.*, 1999; Feig *et al.*, 2007). For the present study, 69 samples were selected from a collective of 700. Their histology was extrapolated from examinations of parallel biopsies from the same testis as part of the routine diagnostic work-up. As a final selection step, results from a test-TESE were taken into account to exclude any discrepancies between the morphological classification of the first biopsy and the spermatogenic activity in a second biopsy from another area of the same testis (compare Feig *et al.*, 2007). Most patients had bilateral biopsies, and care was taken that the selected parallel samples were always from the same side.

RNA preparation

Tissue samples of rice grain size were removed and immediately submerged in RNAlater® (Ambion, Austin, TX, USA). Total RNA was extracted in RNApure™ (Peqlab, Erlangen, Germany) and re-purified on RNeasy™ columns (Qiagen, Hilden, Germany) according to the manufacturers' protocols as described (Feig *et al.*, 2007). Purity and integrity (28S/18S ratio) were assessed by loading 200 ng aliquots onto RNA 6000 nano assay chips using an Agilent Bioanalyzer (Model 2100; Agilent Technologies, Palo Alto, CA, USA). Only samples with an RNA integrity number higher than 7.5 (RIN, Agilent software) were included in the analyses.

Complementary RNA target synthesis and hybridization of Codelink bioarrays

2 μg of total RNA per reaction were employed in reverse transcription as described (Feig *et al.*, 2007). After second-strand synthesis, the complementary DNA (cDNA) served as template for time-optimized *in vitro* transcription using T7 RNA Polymerase to produce target RNA with the CodeLink™ expression assay reagent kit (GE Healthcare, Piscataway, NJ, USA). Concomitant labeling in the presence of biotinylated nucleotides (Biotin-16-UTP, Roche, Switzerland), column-purification, UV spectrophotometry quantification and hybridization to Codelink™ Human 20K Bioarrays (GE Healthcare) was performed as described (Feig *et al.*, 2007). Slides were dried and scanned on a 428™ Array Scanner (Affymetrix, Santa Clara, CA, USA) using Jaguar 2.0 Software. CodeLink™ Expression Analysis Software v4.1 (GE Healthcare) was used for image analysis.

Complementary RNA target synthesis and hybridization of Affymetrix GeneChips

Amplification and biotin labeling of complementary RNA (cRNA) was performed following the Eukaryotic Sample and Array Processing Manual (Affymetrix; Schlecht *et al.*, 2004). Briefly, 2 μg of total RNA were used for reverse transcription using the One-Cycle cDNA Synthesis Kit (Affymetrix). After second-strand synthesis, the cDNA served as template for *in vitro* transcription using the IVT Labeling Kit (Affymetrix) to produce cRNA in the presence of biotin-conjugated nucleotide analogues (16 h, 37°C). Following amplification and purification, cRNA targets were incubated at 94°C for 35 min and the resulting fragments monitored on the BioAnalyzer (Agilent). Hybridization cocktails containing fragmented cRNA at a final concentration of 0.05 μg/μl were transferred into Human Genome U133 Plus 2.0 Array GeneChips (Affymetrix) and incubated for 16 h at 60 U/min at 45°C on a rotator (Affymetrix Hybridization Oven 640). Arrays were washed and stained by using a streptavidine–phycoerythrin conjugate. To increase signal strength, the antibody amplification protocol was used (EukGE-WS2v4; Eukaryotic Sample and Array Processing Manual). GeneChips were processed with a HP GeneArray Scanner (Affymetrix) by using default settings. DAT image files of the microarrays were generated using Microarray Analysis Suite 5.0 (MAS; Affymetrix).

Data analysis and statistics

After elimination of genes below background levels (Codelink: estimated from 300 negative bacterial control spots; GeneChip: the fifth percentile of all expression values) and imputation of missing values by a k-nearest neighbour (KNN) approach (Troyanskaya *et al.*, 2001), datasets were normalized by quantile normalization (*R* package 'affy'). This approach yielded 17 093, 17 949 and 23 822 genes for the Codelink

training and test datasets and for the GeneChip dataset, respectively. In compliance with the MIAME (Minimal Information to Annotate a Microarray Experiment) guidelines (Brazma *et al.*, 2001), raw and processed data files of all specimens were deposited in the Gene Expression Omnibus ('Codelink training set', GSE4797; 'Codelink test set', GSE6023) and ArrayExpress ('GeneChip set', E-TABM-234) public repositories. Defining four morphological subgroups, differential genes were selected by analysis of variance (ANOVA) and the 'Bonferroni' value as the most conservative statistical cut-off (2.93E-6 for Codelink; 2.1E-6 for GeneChip) was employed. Pair-wise individual *t*-tests were performed between the groups in order to elucidate different profiles within the gene list. Hierarchical clustering (average distance, Manhattan metric) was performed on the individual samples or on medians of the subgroups using all genes. Cluster stability was evaluated using multiscale permutation clustering (*R* package 'pvclust'; Suzuki and Shimodaira, 2006). Scaled and centered data were subjected to Principle Component Analysis (PCA, *R* package 'ade4'). The transformed values were additionally analysed using partitioning around medoids (PAM) as implemented in *R* (package 'cluster'). The significance of PAM results after several rounds of analysis using increasing numbers of clusters was verified by using silhouette plots which are to some extent a measure of the degree of similarity of expression patterns in a given cluster compared with all other patterns in the other clusters.

Creation and analysis of the combined data set

Systematic bias reduction was achieved as described by Benito *et al.* (2004) by using the Java implementation of Distance weighted discrimination (DWD) (https://genome.unc.edu/ pubsup/dwd/ DWD.zip). DWD processed datasets were merged and subjected to hierarchical clustering as described above. Stringent classification of all samples was conducted by Diagonal Linear Discriminant Analyis (DLDA), KNN and Support Vector Machines (SVM) using Leave-One-Out-Cross-validation with 2000 permutations of the class labels for a more realistic estimate of the misclassification rate (BRB ArrayTools v.3.4). All scripts used in this analysis can be downloaded from http://humrep.oxfordjournals online.

Quantitative RT–PCR analyses

cDNA synthesis followed standard procedures as described in Feig *et al.* (2007). Primers were designed using free Primer 3 software (http://frodo.wi.mit.edu/); sequences are available as Supplemental information (Supplementary Data S8). Quantitative RT–PCR (qRT–PCR) was performed using LightCycler™ (Roche, Basel, Switzerland) technology. The threshold cycle (crossing point) was determined for each reaction by second derivate maximum method (LightCycler™ Quantification Software). Transcript levels were normalized to ribosomal protein S27 RNA showing minimum variation between individual samples. Fold differences were calculated by use of the relative expression software tool (REST© software, Pfaffl *et al.*, 2002). PCR efficiency was in the range between 1.65 and 1.81 as calculated by an *R* script employing the window-of-linearity method (Ramakers *et al.*, 2003). Products were gel separated and their identity verified by sequence analysis.

Immunohistochemistry

Tissue sections were prepared from Bouin-fixed, paraffin-embedded fragments of testicular biopsies. Anti-calretinin antibody-Zymed, polyclonal from rabbit (Invitrogen, Karlsruhe, Germany) was employed to stain slides at a dilution of 1:100. Antigen localization was achieved using a two-step immunoperoxidase staining method (Envision plus polymer System, DAKO; Hamburg, Germany). Specificity of immunostaining was confirmed by both, omission of primary antibody and staining of parallel sections with antibodies directed against an irrelevant antigen. Stained sections were evaluated by bright-field microscopy (Nikon, Düsseldorf, Germany) and images captured with a Leica DC 300 digital camera (Leitz, Bensheim, Germany).

Counting of mast cells

Testicular mast cell numbers were estimated from 28 diagnostic semithin sections, which had been prepared for diagnostic work-up from plastic-embedded parallel biopsies of the same testes included in the Codelink 28-sample training set. Metachromatic granula-positive cells were counted by two people in four independent fields-of-view in an independent and blinded fashion as described in Jezek *et al.* (1999). Differences between samples from different histological subgroups were calculated with a total of 12 different statistical tests for distribution, location, variance and scale to obtain an overview of the characteristics underlying individual mast cell counts (Supplementary Data S7). In the case of a normal distribution, parametric tests were applied (e.g. *t*-test). In any other case, non-parametric versions of the tests were used (e.g. Wilcoxon rank-sum test).

Over-representation analysis

Over-represented GO (gene ontology) terms and pathways were queried using the DAVID 2007 server (http://niaid.abcc.ncifcrf.gov/). Genes were queried for the over-representation of transcription factor binding sites (TFBS) by using the OPOSSUM web tool version 1.3 (http://www.cisreg.ca/cgi-bin/oPOSSUM/ opossum) with default settings.

Results

Filtering of genes induced in testicular pathology

The 69 analysed biopsies belonged to four distinct histological subtypes termed normal spermatogenesis, uniform hypospermatogenesis, maturation arrest of germ cells at meiosis ('germ cell arrest') and Sertoli-cell-only appearance (compare Feig *et al.*, 2007). Only samples with uniform histology and conformity of test-TESE results were included (see *Materials and Methods*). Cases with obvious morphological differences between individual seminiferous tubules in different areas of the testis were excluded. The sample set contained biopsies from vasectomized men which may exhibit testicular changes (compare Raleigh *et al.*, 2004). However, histological inspection confirmed qualitatively and quantitatively normal spermatogenesis in each of the selected cases, and, importantly, a previous microarray analysis clustered them together with other samples of normal spermatogenesis.

Three sample sets were grouped from the 69 biopsies and individual gene expression patterns assessed in independent laboratories on two microarray platforms. The Codelink training set comprised 28 samples (GSE4797). An equivalent, but independent, GeneChip set comprised 27 samples (E-TABM-234). An additional set of 14 samples was independently analysed on the Codelink platform (GSE6023) and the data included only later as a test set (see below). Comparable analysis procedures were applied to both data sets (see *Materials and Methods*). The overall distributions of ratios from all transcripts were calculated between histological subtypes to assess whether a reduction in germ cell numbers might cause an overall proportional enrichment of somatic

transcripts. This procedure provides more information about changes in cellular distribution compared with a normalization based on erroneously selected somatic genes that might be potentially regulated. Comparing normal spermatogenesis and hypospermatogenesis, a mean ratio near 1 was observed with both platforms (1.05 ± 0.35 and 1.08 ± 0.40, respectively), suggesting that overall changes in transcript proportions were negligible between these subtypes. In comparison, mean ratios of >1 were noticed between normal spermatogenesis and germ cell arrest (1.12 ± 0.48 and 1.24 ± 0.70, respectively), and also between normal spermatogenesis and Sertoli-cell-only appearance (1.35 ± 0.91 and 1.58 ± 1.50, respectively). This observation corroborated histological data indicating such an effect.

To filter the differentially expressed genes, adjusted cut-off values for fold induction were chosen that took into account the effects of non-germ cell enrichment and differences between dynamic range (sensitivities) of the array platforms (Supplementary Fig. S1; compare MAQC consortium, 2006). Using the stringent 'Bonferroni' threshold level for *P*-values (ANOVA) and a fold induction >2 in any one of the three pathological subtypes, 551 differential Codelink genes were filtered which showed significantly increased transcript levels in spermatogenic failure compared with normal spermatogenesis (see Supplementary Data S1). In the GeneChip system, 2096 differential probe sets were filtered which showed a minimum fold induction of 3 (see Supplementary Data S2). The higher number of genes detected by GeneChips can in part be explained by the fact that they covered more genes than the Codelink arrays.

Characteristics of gene expression profiles

Mean transcript levels of differential genes were calculated for each morphological subtype and plotted to illustrate their expression profiles in correlation with these subtypes. The line plots showed similar profiles on both platforms, reflecting a graded induction in correlation with increased spermatogenic damage (Fig. 1, panel A). A significant increase was observed between normal spermatogenesis and hypospermatogenesis, and again between germ cell arrest and Sertoli-cell-only appearance. Maximum transcript levels were most often correlated with Sertoli-cell-only appearance. In hypospermatogenesis and germ cell arrest, fold inductions were often considerably smaller. Quantitative differences between the latter two pathologies, however, were not significant for most loci (Fig. 1, panel B). As a consequence, we were unable to identify any induced genes that discriminated hypospermatogenesis from germ cell arrest with sufficiently high accuracy. We also failed to detect any transcripts which showed significant increase in hypospermatogenesis and/or germ cell arrest, but not in Sertoli-cell-only appearance.

Based on the independent Codelink and GeneChip lists, supervised hierarchical clustering was employed to group the samples in four categories, as suggested from the histological subtypes. Stable clusters of normal spermatogenesis and Sertoli-cell-only appearance were revealed (Supplementary Figs 2 and 3). As opposed to these, samples which showed hypospermatogenesis and germ cell arrest were not clearly separated, but clustered in near vicinity within the dendrograms, pointing to a higher intra-group variability and relatedness in terms of their pathology-induced genes. The tendency of samples to group into three categories instead of four is also illustrated by PCA (Supplementary Figs 2C and 3C).

The PAM cluster algorithm was additionally applied to group the differential GeneChip genes by their similarity of expression profiles in order to possibly identify additional profiles of gene induction. A cluster of 278 Affymetrix probe sets showed a robust increase in the pathological samples (Supplementary Data S3). Again, the individual expression profiles reflected a graded induction of the differential genes, their transcript levels increasing with increased germ cell loss and reaching maximum levels in Sertoli-cell-only appearance. No other PAM clusters of pathology-induced genes were revealed, suggesting that in the histological subtypes studied here, any genes showing divergent profiles of induction were extremely rare, if at all present.

Confirmation of pathology-associated molecular alterations

Linking annotations from both the Codelink and GeneChip lists of differential genes was achieved by conversion into UniGene cluster IDs (UCIDs, Unigene Build #190). An intersection of 188 common UCIDs was apparent (Fig. 2A; Supplementary Data S4). As the differential gene lists had been independently filtered, this overlap validated our results. Based on the PAM algorithm, the number of intersecting genes was smaller, but the overlap was still substantial. When genes from the central most intersection of the Venn diagram were inspected more closely (Fig. 2A), it turned out that they comprised well-known examples of pathology-related genes (compare Table 1) which had previously been shown to be induced in various human pathologies. These genes were characterized by robust fold inductions in all subtypes of defective spermatogenesis, showing ~2-fold increase in expression levels even in hypospermatogenesis (Table 1).

To further validate the array data, qRT–PCR was performed employing cDNAs from all 28 samples of the Codelink training set. Twenty genes were selected from the independent gene lists, comprising known and as yet uncharacterized loci (partially shown in Fig. 3; Supplementary Fig. S4; for oligonucleotide primers, see Supplementary Data S8); in all cases except one (GAK; NM_005255) their increase was confirmed by qRT–PCR. In addition, the profiles obtained by microarray and qRT–PCR expression analyses were in good agreement (Fig. 3). A significant increase of the LH receptor (LHCGR) transcripts was suggested by our data from GeneChips. The gene was not covered by the Codelink array, and thus was not included in the intersection. Still, using the cDNAs from the Codelink samples, the increase was confirmed by qRT–PCR (Fig. 3). Maximum transcript levels of the Leydig cell-specific gene were observed in Sertoli-cell-only appearance; a fold induction clearly above our threshold criteria, however, was also suggested for hypospermatogenesis and germ cell arrest.

Since cell type-specific transcripts are increased as the relative proportion of that specific cell type increases, we looked at genes well known to be specifically expressed in somatic

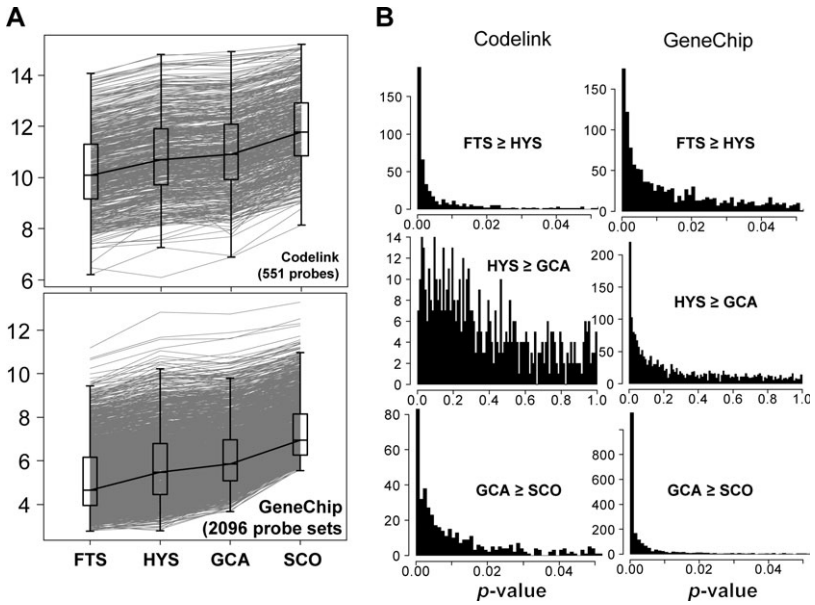

Figure 1: (**A**) Line plots of genes significantly induced in human testicular pathology
Expression profiles of 551 probes (Codelink, upper panel) and 2096 probe sets (GeneChip, lower panel) showed high correlation between increasing transcriptional activity and testicular pathology. Their common characteristic is a statistical significance in the transcriptional changes, which is below the 'Bonferroni' cut-off. The grey lines depict transcriptional profiles, while the black box plots illustrate the median and interquartile ranges from four different pathological subtypes. FTS, full testicular spermatogenesis; GCA, germ cell arrest; HYS, hypospermatogenesis; SCO, Sertoli-cell only. (**B**) *P*-value distribution of all probes (histograms) for the transcriptional changes within FTS/HYS, HYS/GCA and GCA/SCO, respectively, as calculated by *t*-test. Note the high statistical significance of transcriptional changes between FTS and HYS and also between GCA and SCO

testicular cells. Interestingly, many of these were not included in the lists of differentially expressed genes. This group comprised Sertoli cell-specific reference genes such as the Wilms tumour suppressor WT1 (NM_024426), testis-specific kinase TESK2 (NM_007170; Toshima *et al*., 2001), Anti-Müllerian hormone AMH (NM_000479) and the FSH receptor FSHR (NM_000145; compare GSE4797 and E-TABM-234 with Supplementary Data S1 and S2). FSHR transcript levels were confirmed by qRT–PCR (data not shown), suggesting that they were unaffected by impaired or absent sperm production in our patients. Transcript levels of the androgen receptor gene (AR; NM_000044), which is expressed in various somatic cell types of the adult testis, likewise appeared unaffected by the presence or absence of germ cells.

We sought to determine whether increased transcript levels would cause an increase on the protein level. At the same time, we aimed to confirm that the suggested alterations in gene expression affected the somatic testicular cell types. Immunoperoxidase histochemistry (IHC), although not a quantitative method, is currently the only practical way of detecting proteins in small fixed tissue samples. We focused on robust differences in expression levels which might be discerned by IHC and chose calretinin (CALB2 = calbindin 2) as an example (see Table 1; Fig. 4A). Abnormal calretinin expression in azoospermic men had previously been shown by IHC (Bar-Shira Maymon *et al.*, 2005). Employing anti-calretinin antibodies, we compared histological sections of different histological subtypes. Immunostaining of the protein was seen in all subtypes, including normal spermatogenesis, where it appeared to be restricted to the Leydig cells (Fig. 4B), at the same time providing an internal positive control. Sections of biopsies with Sertoli-cell-only appearance revealed an increase in interstitial staining as well as an additional staining within isolated seminiferous tubules (Fig. 4C), most probably originating from Sertoli cells (compare Bar-Shira Maymon *et al.*, 2005).

Functional annotations of pathology-induced genes

Gene annotation enrichment analysis was applied to the lists of differential genes to reveal functional categories over-represented relative to chance (Fig. 2, panel B; Supplementary Data S1–S4). Categories common to both independent Codelink and GeneChip lists included lipid/steroid metabolism, positive regulation of nuclear factor (NF)-κB cascade, focal adhesion and the mitogen-activated protein kinase (MAPK) signalling pathway (Fig. 2, panel B). Over-representation of NF-κB TFBSs in the promoter regions of the induced genes pointed to a potential pathological role of this pro-inflammatory pathway. When only the 188 intersecting genes were considered (compare Supplementary Data S4), over-representation of innate defence and immune response, antigen processing and presentation and NO signalling was observed (Fig. 2, panel B). In the PAM gene list, complement activation, androgen metabolism, innate and humoral immune response, complement and coagulation cascades and xenobiotic metabolism were additional over-represented functional categories.

Annotations and survey of the literature suggested that a considerable proportion of robustly increased transcripts were mast cell-derived. These included TPSAB1 and CPA3, encoding mast cell-specific proteases secreted from the granules upon activation (compare Table 1) and also FCER1G

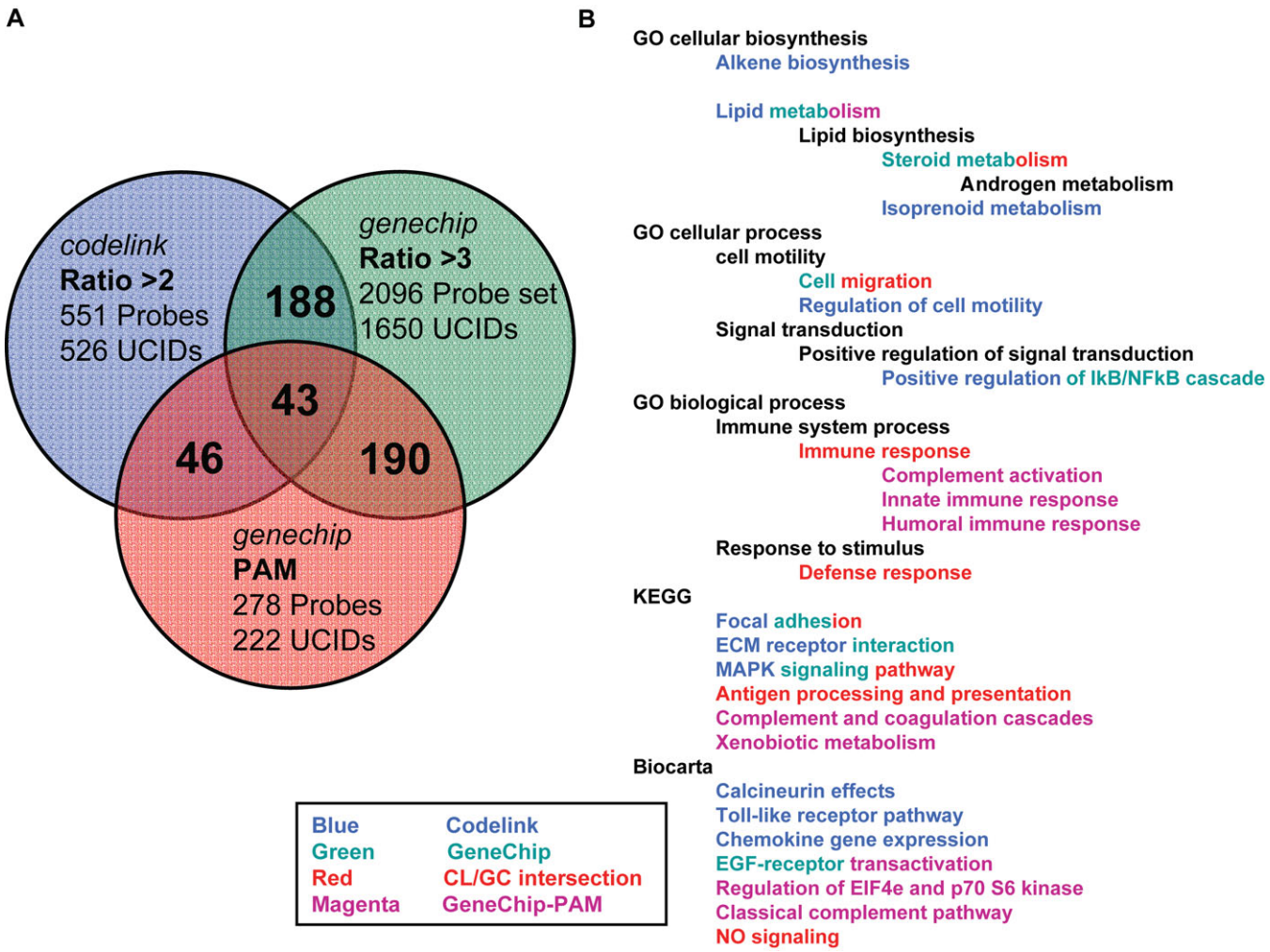

Figure 2: (**A**) Venn diagram showing overlap of genes between three datasets obtained from the Codelink training set, the GeneChip dataset based on the same analytical approach as the former, and a third dataset obtained from supervised partitioning around medoids (PAM) clustering of the GeneChip dataset
'Probes' refers to the differential signals from distinct hybridization probes, UniGene cluster IDs ('UCIDs') to the number of non-redundant UNIGENE clusters. Numbers in intersections refer to common non-redundant UNIGENE clusters. (**B**) Hierarchical representation of Gene Ontology and pathway terms over-represented in the datasets and intersections. Terms in blue, green and magenta are obtained from the Codelink, the GeneChip and the GeneChip PAM analysis, respectively. Common terms of the intersection are in red with underlines. Listed are all terms with *P*-values $P < 0.05$ after multiple testing correction. MAPK, mitogen-activated protein kinase; ECM, extracellular matrix

(NM_004106), encoding the mast cell-specific immunoglobulin (Ig)E-receptor. Additional gene products were contained in the list of differential genes, which had previously been reported to increase in correlation with abnormal activation and/or accumulation of mast cells (and other immune cells). We therefore asked whether certain transcript levels were in keeping with the mast cell numbers in the testicular biopsies. Mast cells are readily detectable as metachromatic granula-positive cells on histological sections (Jezek *et al.*, 1999). They were counted using slides from parallel biopsies to the Codelink samples. Applying parametric or non-parametric statistics, depending on the normal distribution of the cell counts, a significant increase in mast cell number was seen between normal spermatogenesis and Sertoli-cell-only appearance ($P < 0.001$), and further between normal spermatogenesis and hypospermatogenesis ($P < 0.01$; Supplementary Data S7; Supplementary Fig. S5).

To reveal correlations between individual transcript levels and individual numbers of metachromatic granula-positive cells, a logistic regression approach was conducted on each of the 551 differential Codelink genes (Supplementary Data S5). A total of 310 Codelink genes (>60%) were revealed with individual transcript levels correlating directly at $P < 0.05$ with the corresponding metachromatic granula-positive cell numbers. In comparison, when the data were adjusted for individual patients' serum levels of LH, FSH and testosterone as further possible factors which might affect testicular transcript levels, the numbers of genes correlating at the same *P*-value were much lower, i.e. 9, 5 and 28 with individual serum LH, FSH and testosterone levels, respectively.

Cross-platform sample classification

In order to evaluate the potential general significance of the gene expression signature, the expression data of all 69

Table 1: Genes showing robust fold increase (Codelink/GeneChip) between normal spermatogenesis and three subtypes of spermatogenic failure (SCO, GCA and HYS)

Gene abbreviation	Accession number	Name of protein	Functional role (known or assumed); association with disease	Ratio, SCO	Ratio, GCA	Ratio, HYS
CPA3	NM_001870	Carboxypeptidase A3	Mast cell-specific protease; induced in asthma and allergic inflammation	8.64/10.19	2.62/2.08	2.65/1.98
CALB2	NM_001740	Calretinin = Calbindin 2	Calcium-binding protein; cancer-associated, induced upon mast-cell activation and in azoospermia	7.40/6.03	2.75/3.14	1.70/2.70
LDLR	NM_000527	Low density lipoprotein receptor	Lipoprotein binding and endocytosis; dysfunction causes familial hyper-cholesterolemia; increased in inflammation	7.13/3.94	3.54/3.19	3.03/1.90
CLEC2B	NM_005127	C-type lectin domain family 2, member B	Activating receptor; associated with myolocyte/lymphocyte infiltration and activation	5.93/6.57	2.12/3.33	2.13/2.46
TPSAB1	NM_003294	Tryptase alpha/beta	Mast cell-specific protease; induced in inflammation and mast cell-associated fibrosis	5.52/8.71	2.83/2.12	2.02/1.76
SAMD9L	NM_152703	Sterile alpha motif domain containing 9-like	Extraosseous calcification; associated with atherosclerosis and autoimmune disorders	5.24/10.33	1.76/2.46	1.99/1.63
DPT	NM_001937	Dermatopontin	Extracellular matrix protein; increased in fibrotic diseases and infection	4.50/9.09	2.23/3.49	2.12/3.36
RBP1	NM_002899	Cellular retinol binding protein-1 (CRBP1)	Vitamin A homeostasis protein; increased in liver fibrosis/cirrhosis and prostate cancer	4.42/6.21	2.70/2.24	1.97/3.12
CTSC	NM_133504	Cathepsin C = Dipeptidyl peptidase I (DPPI)	Lysosomal protease; increased in sepsis, arthritis, allergic inflammation	4.29/19.99	2.38/3.36	2.17/3.57
ADAMTS5	NM_007038	A disintegrin-like and metalloprotease with thrombospondin type 1 motif, 5	Metalloprotease; involved in degradation of cartilage aggrecan (aggrecanase-2); induced in osteoarthritis	4.09/4.91	2.14/2.34	2.32/1.91
TNFSF13B	NM_006573	Tumour necrosis factor (ligand) superfamily, member 13b (= BAFF)	B cell activating factor; over-expressed in pathogenesis and progression of autoimmune diseases	3.59/7.00	1.70/2.73	1.91/2.13
C1orf24 = FAM129A	NM_052966	NIBAN protein with pleckstrin-homology and armadillo repeat domains	Unknown function; thyroid cancer-associated	3.04/9.64	2.56/6.12	2.34/2.36

GCA, germ cell arrest at meiosis; HYS, hypospermatogenesis; SCO, Sertoli-cell-only appearance.

biopsy samples were merged into a single data set. Gene annotations were converted into UCIDs and multiple occurrences of the same UCID removed by calculating its median value within each experiment and platform. After probe matching, a total of 406 UCIDs was retained from the initially elaborated Codelink list (Supplementary Data S6). To adjust for systematic biases, DWD (Benito *et al.*, 2004) was applied in a pair-wise fashion by first combining the 28-sample Codelink training set with additional 14 samples from the Codelink test set, and then combining this common set with the 27-sample GeneChip data set (Supplementary Fig. S6). Based on the 406 Codelink genes, hierarchical cluster analysis was applied to the integrated data set, resulting in a separation into three categories (Fig. 5, upper panel), similar to the dendrogram structures previously seen in the independent data sets from both platforms (see Supplementary Figs 2 and 3). This implied that the gene expression signature was valid in different sample collectives and patient cohorts which had been assayed with different array platforms.

Referring to the proposals of Dupuy and Simon (2007), we additionally applied three stringent statistical classification methods to the dataset. For this approach, only two alternative categories were distinguished, i.e. 'pathological', comprising hypospermatogenesis, germ cell arrest and Sertoli-cell-only appearance, and 'normal', comprising all samples with quantitatively and qualitatively complete spermatogenesis. Each of DLDA, KNN and SVM was subjected to Leave-One-Out-Cross-validation and 2000 permutations of the class labels in order to obtain a more realistic estimate of the misclassification rate (Fig. 5, lower panel). All Sertoli-cell-only samples ($n = 17$) and all samples with normal spermatogenesis ($n = 21$) were correctly classified. In addition, the majority of samples with hypospermatogenesis and germ cell arrest were correctly classified as 'pathological' samples. In four cases, a misclassification pattern was coherent throughout the different algorithms. In summary, an overall correct sample classification rate of 94.2% was achieved with this more stringent set-up.

Discussion

Microarray data from 69 human testicular biopsies revealed a gene expression signature of spermatogenic failure, which resembled the graded induction of an inflammatory-like response. Approximately 2–3% of testicular transcripts were increased in the pathological samples, their levels gradually growing with the severity of spermatogenic damage and reaching maximum levels in samples with Sertoli-cell-only appearance. As anticipated, germ cell-specific transcripts were not included. These results underscore our previous observation that two fundamentally different patterns of coordinated gene expression

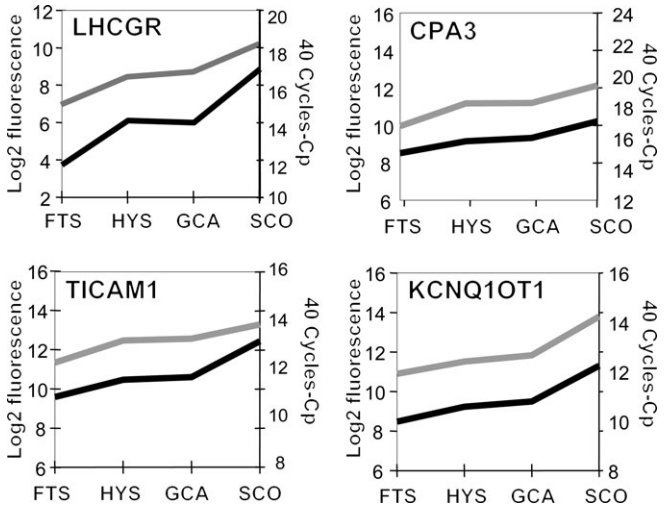

Figure 3: Validation of microarray data by qRT–PCR
A comparison of four selected genes is depicted. Line plots illustrated the good correlation in transcriptional profiles of individual genes obtained from microarray data (black line) and qRT–PCR (grey line). qRT–PCR was applied to the same 28 Codelink samples used for microarray hybridization (with $n = 12, 6, 5, 5$ for the four pathological subtypes, left to right, respectively). The coefficient of variation (c.v.) was under 5% for all samples, hence error bars were omitted in the figure

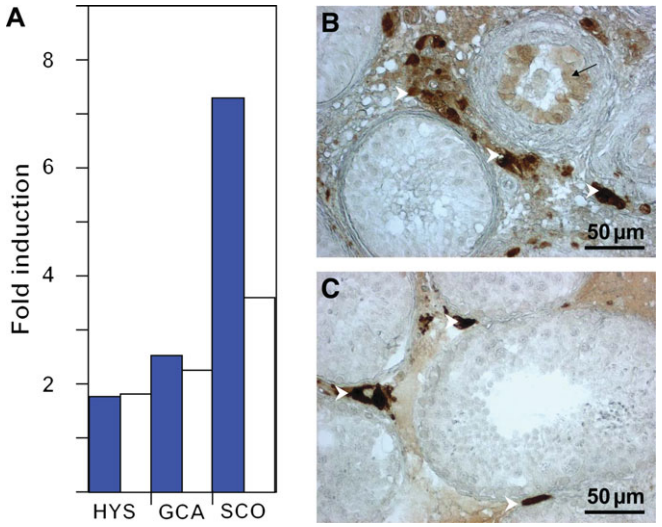

Figure 4: Validation of microarray data for calretinin (=calbindin 2, CALB2) on transcript (**A**) and protein (**B** and **C**) level
(A) qRT–PCR was applied to the same 28 Codelink™ samples as used for microarray hybridization (with $n = 12, 6, 5$ and 5 for the four pathological subtypes, respectively). Box plots showing fold inductions (with respect to FTS) for HYS (Bars 1 and 2), GCA (Bars 3 and 4) and SCO ratios (Bars 5 and 6). Blue: microarray results; white: qRT–PCR results. The c.v. was under 5% for all samples, hence error bars were omitted in the figure. (B) Immunoperoxidase staining using anti-calretinin antibody (1:100) on paraffin-embedded fragment of selected biopsy showing SCO appearance. (C) Immunoperoxidase staining using anti-calretinin antibody (1:100) on paraffin-embedded fragment of selected biopsy showing normal spermatogenesis. White arrowheads point to calretinin immunostaining in interstitium; black arrow points to calretinin staining within seminiferous tubule

are correlated with testicular pathologies (compare Feig *et al.*, 2007). The first and most obvious pattern corresponded to the degree of successful spermatogenesis in each individual sample and comprised predominantly germ cell-specific genes. The second pattern which was analysed here corresponds to pathological changes in testicular non-germ cells. A similar pattern was recently described in human testicular biopsies by Ellis *et al.* (2007) who also observed a pathology-associated increase in transcript levels which corresponded to inflammatory activity. The molecular changes observed in our study were accompanied by extensive tissue remodelling and by an infiltration or activation of immune cells, including mast cells, in the testicular interstitium. Lipid/steroid metabolism, immune response, positive regulation of NF-κB cascade, focal adhesion and MAPK signalling pathway were over-represented functional categories, pathways known to be persistently activated in various other disease states involving inflammation, allergy and autoimmunity (for review, see McCulloch *et al.*, 2006). In the testis, such pathways have been implicated in germ cell apoptosis (Pentikainen *et al.*, 2002; Rasoulpour and Boekelheide, 2007) and ischemia-reperfusion (Lysiak *et al.*, 2005). They may also be a key event in autoimmune orchitis (compare Starace *et al.*, 2005).

Stereological studies in men with impaired spermatogenesis showed altered Leydig cell distribution (Tash *et al.*, 2002; Holm *et al.*, 2003). The proportion of the testis parenchyma occupied by Leydig cells was significantly larger, although the absolute Leydig cell content seemed to be reduced. From our study, increased transcript levels of various Leydig cell markers, including the LHCGR, was suggested, possibly reflecting a proportional increase in Leydig cells in the pathological samples. On the other hand, spermatogenic damage may be associated with impaired Leydig cell functions (Andersson *et al.*, 2004). An increase in Leydig cell markers thus could likewise reflect dysfunction, possibly caused by a disturbed paracrine communication between seminiferous tubules and interstitium which may be ultimately triggered by impaired germ cell functions (for review, see de Kretser, 2004).

Fibrosis of the interstitium and/or fibrotic thickening in the lamina propria is frequently associated with impaired spermatogenesis (de Kretser and Baker, 1996), suggesting that dysregulation of extracellular matrix (ECM) homeostasis is a common feature in human testicular pathology. We observed a robust increase in the pathological samples of transcripts encoding dermatopontin (DPT) and various types of collagen (COL3A1, COL4A6, COL6A3 and COL27A1) which is in line with these observations. *In vitro* studies suggested the basement membrane collagens and mast cell-derived tryptase to be key players in testicular fibrosis, stimulating fibroblast proliferation and increased deposition of ECM material (Frungieri *et al.*, 2002). We found that transcripts encoding mast cell tryptase, mast cell carboxypeptidase, aggrecanase-2 and cathepsin C were significantly induced in all pathological samples. These enzymes are involved in protease-mediated remodelling during pathological and degenerative processes in various tissues and organs (for review, see Laprise *et al.*, 2004; Marshall, 2004; Karsenty, 2005; Hallgren and Pejler, 2006). Enhanced extracellular occurrence in the testis thus would be likely to cause severe tissue damage and/or ECM remodelling.

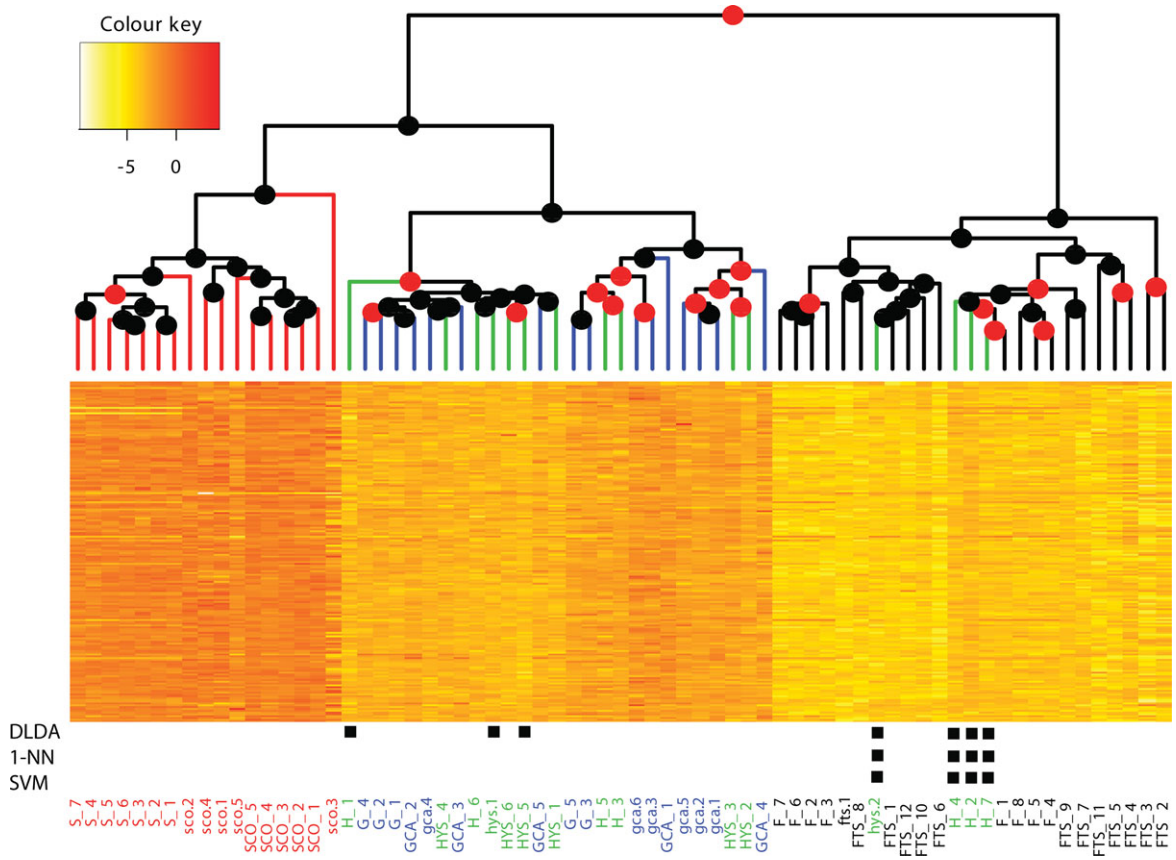

Figure 5: Hierarchical clustering of 406 genes exhibiting pathological up-regulation in the Codelink training set that were extracted from the common set of 8263 genes in both platforms

All 69 samples were hierarchically clustered (Manhattan metric, average distance) using the colour coding as follows. The heat map was built using all genes and heat colours from dark red (high expression) to bright yellow (low expression). Red and black dots on the dendrogram nodes are permutation-based cluster stability *P*-values as calculated from the 'pvclust' package (red: *P*-value ≤ 0.05, black: *P*-value > 0.05). Samples are colour coded in black (FTS, F), green (HYS, H), blue (GCA, G) and red (SCO, S). Sample labels show the origin of the dataset (FTS/HYS/GCA/SCO_X: codelink training; fts/hys/gca/sco.X: codelink test; F/H/G/S_X: geneChip). The bar coding below the heat map was obtained with the 406 genes from a more stringent classification approach using DLDA, 1-NN and SVM, based on 2000 random permutations of the leave-one-out cross-validation misclassification rate. Black boxes show misclassified samples (overall classification rate was 94.2%). DLDA, diagonal linear discriminant analysis; SVM, Support Vector Machines; 1-NN, one-nearest neighbour classification

Immune cells, including mast cells, are normal constituents of the human testis; however, additional cells are recruited in various testicular pathologies (for review, see Fijak and Meinhardt, 2006). In line with a possible infiltration and/or activation of these cells in spermatogenic failure, we see an increase of transcripts encoding the high-affinity IgE receptor (FCER1G; Klemm and Ruland, 2006), components of the inflammasome (PYCARD/ASC and CASP1; for review, see Mariathasan and Monack, 2007), the fractalkine receptor (CX3CR1) which promotes mast cell homing and asthma (Papadopoulos *et al.*, 2000; Laprise *et al.*, 2004), B-cell activating factor (TNFSF13B/ BAFF/BLyS; Claudio *et al.*, 2002), interleukin 32 (IL-32; Conti *et al.*, 2007) as well as NF-κB-activating IL-1 receptor-associated kinase (IRAK1) (Song *et al.*, 2006). Mast cells have been implicated in the pathophysiology of many diverse diseases, operating through the synthesis of pro-inflammatory mediators, the pattern of which varies depending on tissue and stimulus (for review, see Bischoff, 2007). They also contribute to acute testicular inflammation (Iosub *et al.*, 2006). The previous notion that they may also play a role in human testicular physiology and pathology is supported by our results.

Our analysis revealed a common gene expression signature of spermatogenic failure characterized by the graded induction of by and large the same genes in different pathological subgroups, whereby the individual transcript levels closely correlated with degree of spermatogenic damage. Based on these results one might speculate that the different subtypes of human spermatogenic failure represented graded manifestations of a common disorder, which progressively alters the functions (and numbers) of somatic testicular cells and ultimately causes germ cell loss. Conversely, spermatogenic failure and germ cell loss will undoubtedly affect somatic testicular functions. As yet neither the molecular mechanisms are fully understood through which the somatic cells regulate spermatogenesis, nor are the effects of germ cells (or conversely the loss of germ cells) on somatic gene expression. Considering the heterogeneous aetiologies and highly individual molecular causes which may underlie spermatogenic failure in the human, the molecular changes described here may represent common symptoms, but may as well reflect

an inherent dysfunction in the somatic testicular cell types which may causally contribute to the pathology.

In line with this, our microarray results may have clinical implications. They may be useful to develop new diagnostic methods and criteria, provided that increased testicular mRNA levels are accompanied by elevated seminal fluid and/or serum levels of the encoded proteins. As somatic testicular cells are amenable to pharmacological intervention, our results would support anti-inflammatory therapy and/or mast cell inhibition as promising approaches in spermatogenic failure, at least in the less severe cases. Specifically the subgroup of hypospermatogenic men may benefit from such treatments. The results presented by Ellis *et al.* (2007) suggest that they may also be applicable to cases of 'mixed atrophy'. Therapeutically controlling inflammation and/or mast cell functions can significantly improve disease outcomes (McCulloch *et al.*, 2006; Bischoff, 2007), although many patients remained refractory to treatment in the past. Clinical trials in infertility patients have likewise cast doubt on the efficacy of such therapies; however, they may still be effective in a more carefully selected subgroup of patients ('responders'). As probably no single target will be sufficiently effective, the future challenge for therapy design will be to reconcile counteracting regulatory processes which may modulate testicular functions, the NF-κB cascade and other signalling platforms which are activated in defective spermatogenesis representing promising targets.

Supplementary Data

Supplementary data is available at http://humrep.oxfordjournals online.

Acknowledgements

The authors acknowledge the skilled technical assistance of Ms Stefanie Reinhardt. Mr Aleksandar Kibel, University of Osijek, Croatia, helped with the immunohistochemical stainings. The work was generously supported by Drs R. Fischer, O.G.J. Naether and K. Rudolf, Fertility Center Hamburg, Germany, by the German Research Association DFG (contract SP-721/1-1 and SP-721/1-2) and by Serono Deutschland, on behalf of Dr Wilma Bilger. F.C. was supported by the Biozentrum Basel.

References

Alizadeh AA, Eisen MB, Davis RE, Ma C, Lossos IS, Rosenwald A, Boldrick JC, Sabet H, Tran T, Yu X *et al.* Distinct types of diffuse large B-cell lymphoma identified by gene expression profiling. *Nature* 2000;**403**:503–511.

Andersson AM, Jorgensen N, Frydelund-Larsen L, Rajpert-De Meyts E, Skakkebaek NE. Impaired Leydig cell function in infertile men: a study of 357 idiopathic infertile men and 318 proven fertile controls. *J Clin Endocrinol Metab* 2004;**89**:3161–3167.

Bar-Shira Maymon B, Yavetz H, Yogev L, Kleiman SE, Lifschitz-Mercer B, Schreiber L, Botchan A, Hauser R, Paz G. Detection of calretinin expression in abnormal immature Sertoli cells in non-obstructive azoospermia. *Acta Histochem* 2005;**107**:105–112.

Benito M, Parker J, Du Q, Wu J, Xiang D, Perou CM, Marron JS. Adjustment of systematic microarray data biases. *Bioinformatics* 2004;**20**:105–114.

Bischoff SC. Role of mast cells in allergic and non-allergic immune responses: comparison of human and murine data. *Nat Rev Immunol* 2007;**7**:93–104.

Bittner M, Meltzer P, Chen Y, Jiang Y, Seftor E, Hendrix M, Radmacher M, Simon R, Yakhini Z, Ben-Dor A *et al.* Molecular classification of cutaneous malignant melanoma by gene expression profiling. *Nature* 2000;**406**:536–540.

Brazma A, Hingamp P, Quackenbush J, Sherlock G, Spellman P, Stoeckert C, Aach J, Ansorge W, Ball CA, Causton HC *et al.* Minimum information about a microarray experiment (MIAME)-toward standards for microarray data. *Nat Genet* 2001;**29**:365–371.

Claudio E, Brown K, Park S, Wang H, Siebenlist U. BAFF-induced NEMO-independent processing of NF-kappa B2 in maturing B cells. *Nat Immunol* 2002;**3**:958–965.

Conti P, Youinou P, Theoharides TC. Modulation of autoimmunity by the latest interleukins (with special emphasis on IL-32). *Autoimmun Rev* 2007;**6**:131–137.

de Kretser DM. Is spermatogenic damage associated with Leydig cell dysfunction? *J Clin Endocrinol Metab* 2004;**89**:3158–3160. Editorial:.

de Kretser DM, Baker HWG. In: Adashi E Y, Rock JA, Rosenwaks Z (eds). *Reproductive Endocrinology, Surgery, and Technology.* Philadelphia: Lippincott–Raven, 1996, 2031–2062.

Dupuy A, Simon RM. Critical review of published microarray studies for cancer outcome and guidelines on statistical analysis and reporting. *J Natl Cancer Inst* 2007;**99**:147–157.

Ellis PJ, Furlong RA, Conner SJ, Kirkman-Brown J, Afnan M, Barratt C, Griffin DK, Affara NA. Coordinated transcriptional regulation patterns associated with infertility phenotypes in men. *J Med Genet* 2007;**44**:498–508.

Feig C, Kirchhoff C, Ivell R, Naether O, Schulze W, Spiess AN. A new paradigm for profiling testicular gene expression during normal and disturbed human spermatogenesis. *Mol Hum Reprod* 2007;**13**:33–43.

Fijak M, Meinhardt A. The testis in immune privilege. *Immunol Rev* 2006;**213**:66–81.

Fox MS, Ares VX, Turek PJ, Haqq C, Reijo Pera RA. Feasibility of global gene expression analysis in testicular biopsies from infertile men. *Mol Reprod Dev* 2003;**66**:403–421.

Frungieri MB, Weidinger S, Meineke V, Kohn FM, Mayerhofer A. Proliferative action of mast-cell tryptase is mediated by PAR2, COX2, prostaglandins, and PPAR gamma: possible relevance to human fibrotic disorders. *Proc Natl Acad Sci USA* 2002;**99**:15072–15077.

Hallgren J, Pejler G. Biology of mast cell tryptase. An inflammatory mediator. *FEBS J* 2006;**273**:1871–1895.

He Z, Chan WY, Dym M. Microarray technology offers a novel tool for the diagnosis and identification of therapeutic targets for male infertility. *Reproduction* 2006;**132**:11–19.

Holm M, Rajpert-De Meyts E, Andersson AM, Skakkebaek NE. Leydig cell micronodules are a common finding in testicular biopsies from men with impaired spermatogenesis and are associated with decreased testosterone/LH ratio. *J Pathol* 2003;**199**:378–386.

Iosub R, Klug J, Fijak M, Schneider E, Fröhlich S, Blumbach K, Wennemuth G, Sommerhoff CP, Steinhoff M, Meinhardt A. Development of testicular inflammation in the rat involves activation of proteinase-activated receptor-2. *J Pathol* 2006;**208**:686–698.

Jezek D, Banek L, Hittmair A, Pezerovic-Panijan R, Goluza T, Schulze W. Mast cells in testicular biopsies of infertile men with mixed atrophy of seminiferous tubules. *Andrologia* 1999;**31**:203–210.

Jezek D, Knuth UA, Schulze W. Successful testicular sperm extraction (TESE) in spite of high serum follicle stimulating hormone and azoospermia: correlation between testicular morphology, TESE results, semen analysis and serum hormone values in 103 infertile men. *Hum Reprod* 1998;**13**:1230–1234.

Karsenty G. An aggrecanase and osteoarthritis. *N Engl J Med* 2005;**353**:522–523.

Klemm S, Ruland J. Inflammatory signal transduction from the Fc epsilon RI to NF-kappaB. *Immunobiology* 2006;**211**:815–820.

Laprise C, Sladek R, Ponton A, Bernier MC, Hudson TJ, Laviolette M. Functional classes of bronchial mucosa genes that are differentially expressed in asthma. *BMC Genomics* 2004;**5**:21–31.

Lysiak JJ, Bang HJ, Nguyen QA, Turner TT. Activation of the nuclear factor kappa B pathway following ischemia-reperfusion of the murine testis. *J Androl* 2005;**26**:129–135.

MAQC Consortium, Shi L, Reid LH, Jones WD, Shippy R, Warrington JA, Baker SC, Collins PJ, de Longueville F, Kawasaki ES, Lee KY *et al.* The MicroArray Quality Control (MAQC) project shows inter- and intraplatform reproducibility of gene expression measurements. *Nat Biotechnol* 2006;**24**:1151–1161.

Mariathasan S, Monack DM. Inflammasome adaptors and sensors: intracellular regulators of infection and inflammation. *Nat Rev Immunol* 2007;**7**:31–40.

Marshall JS. Mast-cell responses to pathogens. *Nat Rev Immunol* 2004;**4**: 787–799.

McCulloch CA, Downey GP, El-Gabalawy H. Signalling platforms that modulate the inflammatory response: new targets for drug development. *Nat Rev Drug Discov* 2006;**5**:864–876.

McLachlan RI, Rajpert-De Meyts E, Hoei-Hansen CE, de Kretser DM, Skakkebaek NE. Histological evaluation of the human testis—approaches to optimizing the clinical value of the assessment: mini review. *Hum Reprod* 2007;**22**:2–16.

Papadopoulos EJ, Fitzhugh DJ, Tkaczyk C, Gilfillan AM, Sassetti C, Metcalfe DD, Hwang ST. Mast cells migrate, but do not degranulate, in response to fractalkine, a membrane-bound chemokine expressed constitutively in diverse cells of the skin. *Eur J Immunol* 2000;**30**: 2355–2361.

Pentikainen V, Suomalainen L, Erkkila K, Martelin E, Parvinen M, Pentikainen MO, Dunkel L. Nuclear factor-kappa B activation in human testicular apoptosis. *Am J Pathol* 2002;**160**:205–218.

Perou CM, Sorlie T, Eisen MB, van de Rijn M, Jeffrey SS, Rees CA, Pollack JR, Ross DT, Johnsen H, Akslen LA *et al.* Molecular portraits of human breast tumours. *Nature* 2000;**406**:747–752.

Pfaffl MW, Horgan GW, Dempfle L. Relative expression software tool (REST) for group-wise comparison and statistical analysis of relative expression results in real-time PCR. *Nucleic Acids Res* 2002;**30**:e36.

Raleigh D, O'Donnell L, Southwick GJ, de Kretser DM, McLachlan RI. Stereological analysis of the human testis after vasectomy indicates impairment of spermatogenic efficiency with increasing obstructive interval. *Fertil Steril* 2004;**81**:1595–1603.

Ramakers C, Ruijter JM, Deprez RH, Moorman AF. Assumption-free analysis of quantitative real-time polymerase chain reaction (PCR) data. *Neurosci Lett* 2003;**339**:62–66.

Rasoulpour RJ, Boekelheide K. NF-kappaB activation elicited by ionizing radiation is proapoptotic in testis. *Biol Reprod* 2007;**76**: 279–285.

Rockett JC, Patrizio P, Schmid JE, Hecht NB, Dix DJ. Gene expression patterns associated with infertility in humans and rodent models. *Mutat Res* 2004;**549**:225–240.

Schlecht U, Demougin P, Koch R, Hermida L, Wiederkehr C, Descombes P, Pineau C, Jegou B, Primig M. Expression profiling of mammalian male meiosis and gametogenesis identifies novel candidate genes for roles in the regulation of fertility. *Mol Biol Cell* 2004;**15**:1031–1043.

Schulze W, Thoms F, Knuth UA. Testicular sperm extraction: comprehensive analysis with simultaneously performed histology in 1418 biopsies from 766 subfertile men. *Hum Reprod* 1999;**14**(Suppl 1):82–96.

Song YJ, Jen KY, Soni V, Kieff E, Cahir-McFarland E. IL-1 receptor-associated kinase 1 is critical for latent membrane protein 1-induced p65/RelA serine 536 phosphorylation and NF-kappaB activation. *Proc Natl Acad Sci USA* 2006;**103**:2689–2694.

Starace D, Riccioli A, D'Alessio A, Giampietri C, Petrungaro S, Galli R, Filippini A, Ziparo E, De Cesaris P. Characterization of signaling pathways leading to Fas expression induced by TNF-alpha: pivotal role of NF-kappaB. *FASEB J* 2005;**19**:473–475.

Suzuki R, Shimodaira H. Pvclust: an R package for assessing the uncertainty in hierarchical clustering. *Bioinformatics* 2006;**22**:1540–1542.

Tash JA, McCallum S, Hardy MP, Knudsen B, Schlegel PN. Men with nonobstructive azoospermia have Leydig cell hypertrophy but not hyperplasia. *J Urol* 2002;**168**:1068–1070.

Toshima J, Toshima JY, Takeuchi K, Mori R, Mizuno K. Cofilin phosphorylation and actin reorganization activities of testicular protein kinase 2 and its predominant expression in testicular Sertoli cells. *J Biol Chem* 2001;**276**:31449–31458.

Troyanskaya O, Cantor M, Sherlock G, Brown P, Hastie T, Tibshirani R, Botstein D, Altman RB. Missing value estimation methods for DNA microarrays. *Bioinformatics* 2001;**17**:520–525.

Yamanaka K, Fujisawa M, Tanaka H, Okada H, Arakawa S, Kamidono S. Significance of human testicular mast cells and their subtypes in male infertility. *Hum Reprod* 2000;**15**:1543–1547.

Yang B, Wang H, Gao XK, Chen BQ, Zhang YQ, Liu HL, Wang Y, Qin WJ, Qin RL, Shao GX *et al.* Expression and significance of Rap1A in testes of azoospermic subjects. *Asian J Androl* 2004;**6**:35–40.

Submitted on May 15, 2007; resubmitted on July 19, 2007; accepted on August 1, 2007